Several Compact Local Stencils based on Integrated RBFs for Fourth-Order ODEs and PDEs

T.-T. Hoang-Trieu[1], N. Mai-Duy[1] and T. Tran-Cong[1]

Abstract: In this paper, new compact local stencils based on integrated radial basis functions (IRBFs) for solving fourth-order ordinary differential equations (ODEs) and partial differential equations (PDEs) are presented. Five types of compact stencils - 3-node and 5-node for 1D problems and 5×5-node, 13-node and 3×3 -node for 2D problems - are implemented. In the case of 3-node stencil and 3×3-node stencil, nodal values of the first derivative(s) of the field variable are treated as additional unknowns (i.e. 2 unknowns per node for 3-node stencil and 3 unknowns per node for 3×3-node stencil). The integration constants arising from the construction of IRBFs are exploited to incorporate into the local IRBF approximations (i) values of the governing equation (GE) at selected nodes for the case of 5-, 5×5- and 13-node stencils, and (ii) not only nodal values of the governing equation but also nodal values of the first derivative(s) for the case of 3-node stencil and 3×3-node stencil. There are no special treatments required for grid nodes near the boundary for 3-node stencil and 3×3-node stencil. The proposed stencils, which lead to sparse system matrices, are numerically verified through the solution of several test problems.

Keywords: Compact local approximations, high-order ODEs, high-order PDEs, integrated radial basis functions.

1   Introduction

Numerical techniques have been developed to solve ODEs and PDEs which are used to model continuum mechanics problems such as the motion of a fluid and the deformation of a solid body. Traditional discretisation methods include finite-difference methods (FDMs) [Conte and Dames (1958); Smith (1978); Gupta and Manohar (1979); Bjørstad (1983)], finite-element methods (FEMs) [Reddy (2005); Hughes (1987); Rannacher (1999)], boundary-element methods (BEMs) and finite-

[1] Computational Engineering and Science Research Centre, Faculty of Engineering and Surveying, University of Southern Queensland, Toowoomba, QLD 4350, Australia.

volume methods (FVMs) [Patankar (1980)]. Over the last 20 years, RBFs, which are known as a universal approximator, have been applied for the solution of ODEs and PDEs [Franke (1982); Kansa (1990a,b); Haykin (1999); Kansa (1999)]. They were first developed as a global technique, in which the dependent variable is decomposed into a set of RBFs defined over the whole domain of analysis, and its derivatives are then calculated through differentiation (differentiated RBFs (DRBFs)). Later on, Mai-Duy and Tran-Cong [Mai-Duy and Tran-Cong (2001, 2003); Mai-Duy (2005); Mai-Duy and Tanner (2005b)] proposed integrated RBF (IRBF) methods, in which highest-order derivative(s) in the ODE/PDE are approximated by RBFs, and lower-order derivatives and the dependent variable itself are then obtained by integration. Numerical results showed that IRBFs yield better accuracy than DRBFs.

Global IRBF methods have some strengths and weaknesses. They can produce very accurate solutions using relatively low numbers of data nodes, and their implementations are quite straightforward. However, they lead to fully populated system matrices. As a result, for a given spatial discretisation, global IRBF methods require larger computer storage than traditional methods. In addition, their matrix condition number grows very quickly as the number of nodes increases. To overcome these drawbacks, local and compact local IRBF schemes have been developed (e.g. [Mai-Duy and Tran-Cong (2009); Ngo-Cong, Mai-Duy, Karunasena, and Tran-Cong (2010); An-Vo, Mai-Duy, and Tran-Cong (2011); Mai-Duy and Tran-Cong (2011)]). Such local schemes result in sparse system matrices and a solution to an algebraic set of equations is thus more efficient. In [Mai-Duy and Tran-Cong (2011)], compact local IRBF stencils for solving second-order ODEs with Dirichlet and Neumann boundary conditions, and second-order PDEs (i.e. Poisson equation) on rectangular and non-rectangular domains were proposed; it was observed that compact local forms produce much more accurate results than local forms and also than global 1D-IRBF forms in some cases.

This paper is concerned with the development of compact local IRBF stencils for the solution of fourth-order ODEs and PDEs. The following two strategies (e.g. [Stephenson (1984); Altas, Dym, Gupta, and Manohar (1998)]) are studied in the context of local compact IRBFs.

The first strategy employs relatively large stencils (i.e. 5 nodes for 1D fourth-order problems, and 13 nodes or 5×5 nodes for 2D fourth-order problems). For this approach, only nodal values of the field variable on a stencil are treated as unknowns. It is noted that, when compared with second-order problems, there are more nodes used on a stencil (i.e. 2 additional nodes for 1D problems, and 4 and 16 additional nodes for 2D problems).

The second strategy employs relatively small stencils (i.e. 3 nodes for 1D prob-

lems and 3×3 nodes for 2D problems). For this approach, not only nodal values of the field variable on a stencil but also nodal values of its first derivative at selected nodes are treated as unknowns. Advantages of this strategy include (i) the number of nodes employed here does not increase when compared with the case of second-order problems; (ii) there are no special treatments required for grid nodes near the boundary; (iii) derivative boundary values can be imposed easily and accurately; and (iv) first derivative values are obtained directly from the final system of algebraic equations.

Furthermore, in both strategies, we also incorporate nodal values of the governing equation at selected nodes on a stencil into the IRBF approximations. Numerical results will show that such an incorporation can significantly enhance the solution accuracy.

The remainder of the paper is organised as follows. Section 2 is a brief review of IRBFs. The proposed compact local stencils based on IRBFs are presented for 1D problems in Section 3 and for 2D problems in Section 4. Numerical examples are given in Section 5 to demonstrate the attractiveness of the proposed stencils. Section 6 concludes the paper.

2 Brief review of integrated RBFs

Consider a continuous function $u(\mathbf{x})$ where $\mathbf{x}$ is the position vector. Such a function can be approximated using integrated RBF schemes of second and fourth orders.

2.1 Second-order integrated RBF scheme

In this scheme, the second-order derivatives of the function u are decomposed into a set of RBFs

$$\frac{\partial^2 u(\mathbf{x})}{\partial \eta^2} = \sum_{i=1}^{n} w_i I_i^{(2)}(\eta), \tag{1}$$

where η denotes a component of the position vector $\mathbf{x}$ (e.g. η can be x for 1D problems, and x or y for 2D problems), $\{w_i\}_{i=1}^{n}$ is the set of RBF coefficients which are unknown, and $\left\{ I_i^{(2)}(\eta) \right\}_{i=1}^{n}$ is the set of RBFs. Expression (1) is then integrated to obtain approximate expressions for lower order derivatives and the function itself as follows.

$$\frac{\partial u(\mathbf{x})}{\partial \eta} = \sum_{i=1}^{n} w_i I_i^{(2)}(\eta) + c_1, \tag{2}$$

$$u(\mathbf{x}) = \sum_{i=1}^{n} w_i I_i^{(0)}(\eta) + \eta c_1 + c_2, \tag{3}$$

where c_1 and c_2 are "constants of integration" with respect to η, which are to be treated as the additional RBF coefficients. In (1)-(3), the superscript (.) is used to indicate the associated derivative order.

Collocating (1)-(3) at a set of nodal points $\{\mathbf{x}_i\}_{i=1}^n$ yields

$$\widehat{\frac{\partial^2 u}{\partial \eta^2}} = \mathscr{H}_\eta^{(2)} \widehat{w}_\eta, \tag{4}$$

$$\widehat{\frac{\partial u}{\partial \eta}} = \mathscr{H}_\eta^{(1)} \widehat{w}_\eta, \tag{5}$$

$$\widehat{u} = \mathscr{H}_\eta^{(0)} \widehat{w}_\eta, \tag{6}$$

where the notation $\frown$ is used to denote a vector, $\mathscr{H}^{(\cdot)}$ is the RBF coefficient matrix in the RBF space and $\widehat{w}_\eta$ is the RBF vector of coefficients, including the integration constants.

2.2   Fourth-order integrated RBF scheme

In this scheme, the fourth-order derivatives of the function u are decomposed into a set of RBFs as

$$\frac{\partial^4 u(\mathbf{x})}{\partial \eta^4} = \sum_{i=1}^n w_i I_i^{(4)}(\eta). \tag{7}$$

Approximate expressions for lower order derivatives and the function itself are then obtained through integration as

$$\frac{\partial^3 u(\mathbf{x})}{\partial \eta^3} = \sum_{i=1}^n w_i I_i^{(3)}(\eta) + c_1, \tag{8}$$

$$\frac{\partial^2 u(\mathbf{x})}{\partial \eta^2} = \sum_{i=1}^n w_i I_i^{(2)}(\eta) + \eta c_1 + c_2, \tag{9}$$

$$\frac{\partial u(\mathbf{x})}{\partial \eta} = \sum_{i=1}^n w_i I_i^{(1)}(\eta) + \frac{\eta^2}{2} c_1 + \eta c_2 + c_3, \tag{10}$$

$$u(\mathbf{x}) = \sum_{i=1}^n w_i I_i^{(0)}(\eta) + \frac{\eta^3}{6} c_1 + \frac{\eta^2}{2} c_2 + \eta c_3 + c_4. \tag{11}$$

Collocating (7)-(11) at a set of nodal points $\{\mathbf{x}_i\}_{i=1}^{n}$ yields

$$\widehat{\frac{\partial^4 u}{\partial \eta^4}} = \mathscr{H}_{\eta}^{(4)} \widehat{w}_{\eta}, \tag{12}$$

$$\widehat{\frac{\partial^3 u}{\partial \eta^3}} = \mathscr{H}_{\eta}^{(3)} \widehat{w}_{\eta}, \tag{13}$$

$$\widehat{\frac{\partial^2 u}{\partial \eta^2}} = \mathscr{H}_{\eta}^{(2)} \widehat{w}_{\eta}, \tag{14}$$

$$\widehat{\frac{\partial u}{\partial \eta}} = \mathscr{H}_{\eta}^{(1)} \widehat{w}_{\eta}, \tag{15}$$

$$\widehat{u} = \mathscr{H}_{\eta}^{(0)} \widehat{w}_{\eta}. \tag{16}$$

For the approximations of integration constants used in (1)-(3) and (7)-(11), the reader is referred to [Mai-Duy and Tran-Cong (2003, 2010)] for further details.

In this study, the multiquadric (MQ) function is chosen as the basis function as

$$I_i^{(4)}(x) = \sqrt{(x-c_i)^2 + a_i^2} \quad \text{for 1D problems,} \tag{17}$$

$$I_i^{(4)}(\mathbf{x}) = \sqrt{(x-c_{ix})^2 + (y-c_{iy})^2 + a_i^2} \quad \text{for 2D problems,} \tag{18}$$

where c_i (for 1D problems) or $(c_{ix}, c_{iy})^T$ (for 2D problems) and a_i are the MQ centre and width, respectively. The width of the ith MQ can be determined according to the following relation

$$a_i = \beta d_i, \tag{19}$$

where β is a factor ($\beta > 0$) and d_i is the distance from the ith centre to the nearest neighbour. It was observed in [Kansa (1990a)] that, as the RBF width increases, the numerical error of the RBF solution reduces and the condition number of the interpolant grows. At large values of β, one needs to pay special attention as the solution becomes unstable. Reported values of β vary from, typically, 1 for global IRBF methods to a wide range of $2 - 200$ for local and compact local IRBF methods. For the latter, one can vary the value of β and/or refine the spatial discretisation to enhance the solution accuracy.

In the following sections, to simplify the notations, we will drop out the subscript η used in (12)-(16) for 1D problems, and use (i, j) to represent a grid node located at (x_i, y_j) in a global 2D grid, $\mathbf{x}_k$ to represent a grid node k in a local 2D stencil, and $\mathscr{M}(i,:)$ to denote the ith row of the matrix $\mathscr{M}$.

3   Proposed compact local IRBF stencils for fourth-order ODEs

Our sample of fourth-order ODEs is taken as

$$\frac{d^4u}{dx^4} + \frac{d^2u}{dx^2} = f(x), \tag{20}$$

where $x_A \leq x \leq x_B$ and $f(x)$ is some given function. The boundary conditions prescribed here are of Dirichlet type, i.e. u and du/dx given at both x_A and x_B.

We discretise the problem domain using a set of n discrete nodes $\{x_i\}_{i=1}^n$, and utilise fourth-order IRBF schemes to represent the field variable u.

3.1   Compact local 5-node stencil (5-node CLS)

Consider a grid node x_i and its associated 5-node stencil $[x_1^i, x_2^i, x_3^i, x_4^i, x_5^i]$ $(x_i \equiv x_3^i)$.

The conversion system, which represents the relation between the RBF space and the physical space, is established from the following equations

$$\begin{pmatrix} \widehat{u} \\ \widehat{e} \end{pmatrix} = \underbrace{\begin{bmatrix} \mathscr{H}^{(0)} \\ \mathscr{K} \end{bmatrix}}_{\mathscr{C}} \widehat{w}, \tag{21}$$

where $\mathscr{C}$ is the conversion matrix, $\widehat{u} = (u_1, u_2, u_3, u_4, u_5)^T$, $\widehat{w} = (w_1, w_2, w_3, w_4, w_5, c_1, c_2, c_3, c_4)^T$, $\widehat{u} = \mathscr{H}^{(0)}\widehat{w}$ are equations representing nodal values of u over the stencil, $\mathscr{H}^{(0)}$ is a 5×9 matrix that is obtained from collocating (11) at grid nodes of the stencil, $\widehat{e} = \mathscr{K}\widehat{w}$ are equations representing extra information that can be the ODE (20) at selected nodes, and du/dx at x_A and x_B. Solving (21) results in

$$\widehat{w} = \mathscr{C}^{-1} \begin{pmatrix} \widehat{u} \\ \widehat{e} \end{pmatrix}. \tag{22}$$

If the number of extra information values are less than or equal to 4, the obtained conversion matrix in (21) is not overdetermined owing to the presence of the integration constants. In this case, the extra information is thus imposed in an exact manner. By substituting (22) into (7)-(11), values of u and its derivatives at an

arbitrary point x on the stencil are calculated in the physical space as

$$\frac{d^4 u(x)}{x^4} = \left[\begin{array}{cccccc} I_1^{(4)}(x), & \ldots, & I_5^{(4)}(x), & 0, & 0, & 0, & 0 \end{array} \right] \mathscr{C}^{-1} \left(\begin{array}{c} \widehat{u} \\ \widehat{e} \end{array} \right), \qquad (23)$$

$$\frac{d^3 u(x)}{dx^3} = \left[\begin{array}{cccccc} I_1^{(3)}(x), & \ldots, & I_5^{(3)}(x), & 1, & 0, & 0, & 0 \end{array} \right] \mathscr{C}^{-1} \left(\begin{array}{c} \widehat{u} \\ \widehat{e} \end{array} \right), \qquad (24)$$

$$\frac{d^2 u(x)}{dx^2} = \left[\begin{array}{cccccc} I_1^{(2)}(x), & \ldots, & I_5^{(2)}(x), & x, & 1, & 0, & 0 \end{array} \right] \mathscr{C}^{-1} \left(\begin{array}{c} \widehat{u} \\ \widehat{e} \end{array} \right), \qquad (25)$$

$$\frac{du(x)}{dx} = \left[\begin{array}{cccccc} I_1^{(1)}(x), & \ldots, & I_5^{(1)}(x), & x^2/2, & x, & 1, & 0 \end{array} \right] \mathscr{C}^{-1} \left(\begin{array}{c} \widehat{u} \\ \widehat{e} \end{array} \right), \qquad (26)$$

$$u(x) = \left[\begin{array}{cccccc} I_1^{(0)}(x), & \ldots, & I_5^{(0)}(x), & x^3/6, & x^2/2, & x, & 1 \end{array} \right] \mathscr{C}^{-1} \left(\begin{array}{c} \widehat{u} \\ \widehat{e} \end{array} \right). \qquad (27)$$

where $x_1^i \le x \le x_5^i$. In what follows, we present two ways to construct the final system of algebraic equations, namely Implementation 1 and Implementation 2.

Implementation 1: The final system is generated by

(i) the collocation of the ODE (20) at $\{x_3, x_4, \ldots, x_{n-2}\}$ using (23) and (25) with $x = x_i$, in which $\widehat{e} = \mathscr{K}\widehat{w}$ is employed to represent values of (20) at x_2^i and x_4^i, i.e.

$$\left(\begin{array}{c} f\left(x_2^i\right) \\ f\left(x_4^i\right) \end{array} \right) = \left[\begin{array}{c} \mathscr{G}(2,:) \\ \mathscr{G}(4,:) \end{array} \right] \widehat{w}, \qquad (28)$$

where $\mathscr{G} = \mathscr{H}^{(4)} + \mathscr{H}^{(2)}$, and

(ii) the imposition of du/dx at x_A and x_B using (26) with $x = x_1$ and $x = x_n$.

Implementation 2: The final system is generated by collocating the ODE (20) at $\{x_4, x_5, \ldots, x_{n-3}\}$ and $\{x_2, x_3, x_{n-2}, x_{n-1}\}$. For the former, the collocation process is similar to that of Implementation 1. For the latter, special treatments for the imposition of first derivative boundary conditions are required. Collocations of the ODE (20) at $\{x_2, x_3\}$ and $\{x_{n-2}, x_{n-1}\}$ are based on the stencils of nodes x_3 and x_{n-2}, respectively, with the following modified extra information vectors
$\widehat{e} = (du(x_1^i)/dx, f(x_4^i))^T$ for the stencil of x_3,
$\widehat{e} = (f(x_2^i), du(x_5^i)/dx)^T$ for the stencil of x_{n-2}.
Both implementations lead to a system matrix of dimensions $(n-2) \times (n-2)$.

3.2 Compact local 3-node stencil (3-node CLS)

Consider a grid node x_i $(i = \{2, 3, \ldots, n-1\})$ with its associated 3-node stencil $[x_1^i, x_2^i, x_3^i]$ $(x_i \equiv x_2^i)$.

Unlike the CL 5-node stencil, nodal values of the first derivative of the field variable are also treated here as unknowns. There are thus two unknowns, namely u and du/dx, per node.

We form the conversion system as follows.

$$
\begin{pmatrix} \widehat{u} \\ \widehat{du} \\ \widehat{e} \end{pmatrix} = \underbrace{\left[\begin{array}{c} \mathscr{H}^{(0)} \\ \mathscr{H}^{(1)} \\ \mathscr{K} \end{array} \right]}_{\mathscr{C}} \widehat{w},
\tag{29}
$$

where $\mathscr{C}$ is the conversion matrix, $\widehat{u} = (u_1, u_2, u_3)^T$, $\widehat{du} = \left(du(x_1^i)/dx, du(x_3^i)/dx \right)^T$, $\widehat{w} = (w_1, w_2, w_3, c_1, c_2, c_3, c_4)^T$, $\widehat{u} = \mathscr{H}^{(0)} \widehat{w}$ is a set of three equations representing nodal values of u over the stencil, $\widehat{du} = \mathscr{H}^{(1)} \widehat{w}$ is a set of two equations representing nodal values of the first derivative at x_1^i and x_3^i, and $\widehat{e} = \mathscr{K} \widehat{w}$ is a set of equations which can be used to incorporate more information into the approximations.

Solving (29) results in

$$
\widehat{w} = \mathscr{C}^{-1} \begin{pmatrix} \widehat{u} \\ \widehat{du} \\ \widehat{e} \end{pmatrix}.
\tag{30}
$$

It can be seen that the IRBF approximations for the field variable and its derivatives can now be expressed in terms of not only nodal values of u at the three grid nodes of the stencil but also nodal values of du/dx at the two extreme nodes of the stencil.

The two unknowns at the central point of the stencil (x_2^i) require the establishment of two algebraic equations. This can be achieved by collocating the ODE (20) at x_2^i and collocating the first derivative at x_2^i

$$
f(x_2^i) = \mathscr{G}(2,:)\mathscr{C}^{-1} \begin{pmatrix} \widehat{u} \\ \widehat{du} \\ \widehat{e} \end{pmatrix},
\tag{31}
$$

$$
\frac{du(x_2^i)}{dx} = \mathscr{H}^{(1)}(2,:)\,\mathscr{C}^{-1} \begin{pmatrix} \widehat{u} \\ \widehat{du} \\ \widehat{e} \end{pmatrix},
\tag{32}
$$

where $\mathscr{G} = \mathscr{H}^{(4)} + \mathscr{H}^{(2)}$.

The above process leads to a determined final system with $(n-2)$ equations for the ODE, $(n-2)$ equations for the first derivative du/dx, $(n-2)$ unknowns for the field variable u and $(n-2)$ unknowns for du/dx at the interior nodes.

In the case that $\widehat{e}$ is used to represent the governing equation (GE) (20) at x_1^i and x_3^i, i.e.

$$\underbrace{\begin{pmatrix} f(x_1^i) \\ f(x_3^i) \end{pmatrix}}_{\widehat{e}} = \begin{pmatrix} \mathscr{G}(1,:) \\ \mathscr{G}(3,:) \end{pmatrix} \widehat{w}, \tag{33}$$

we name the corresponding stencil a 3-node CLS with GE.

In the case that $\widehat{e}$ is simply set to null, we call it a 3-node CLS without GE.

4 Proposed compact local IRBF stencils for fourth-order PDEs

Consider a 2D fourth-order differential problem governed by the biharmonic equation

$$\frac{\partial^4 u}{\partial x^4} + 2\frac{\partial^4 u}{\partial x^2 y^2} + \frac{\partial^4 u}{\partial y^4} = f(x,y) \tag{34}$$

on a rectangular domain ($x_A \leq x \leq x_B$, $y_C \leq y \leq y_D$), and subject to Dirichlet boundary conditions (i.e. u and $\partial u/\partial n$ given at the boundaries (n the normal direction)).

The problem domain is represented by a Cartesian grid of $n_x \times n_y$ as shown in Figure 1. We employ fourth-order IRBF schemes for compact local 5×5-node and 13-node stencils, and second-order IRBF schemes for compact local 3×3-node stencils.

4.1 *Compact local* 5×5-*node stencil (5×5-node CLS)*

Consider a grid node (i,j) and its associated 5×5-node stencil. The stencil is locally numbered from left to right and from bottom to top (node $(i,j) \equiv$ node 13) (Figure 2). The solution procedure here is similar to that for 1D problems. However, the 2D problem formulation involves more terms and requires special treatments for interior "corner" nodes.

The conversion system is constructed as

$$\begin{pmatrix} \widehat{u} \\ \widehat{0} \\ \widehat{e} \end{pmatrix} = \underbrace{\begin{bmatrix} \mathscr{H}_x^{(0)}, & \mathscr{O} \\ \mathscr{H}_x^{(0)}, & -\mathscr{H}_y^{(0)} \\ \mathscr{K}_x, & \mathscr{K}_y \end{bmatrix}}_{\mathscr{C}} \begin{pmatrix} \widehat{w}_x \\ \widehat{w}_y \end{pmatrix}, \tag{35}$$

where the subscripts x and y denote the quantity associated with the integration process in the x and y direction, respectively; $\widehat{0}$ and $\mathscr{O}$ are a vector and a matrix
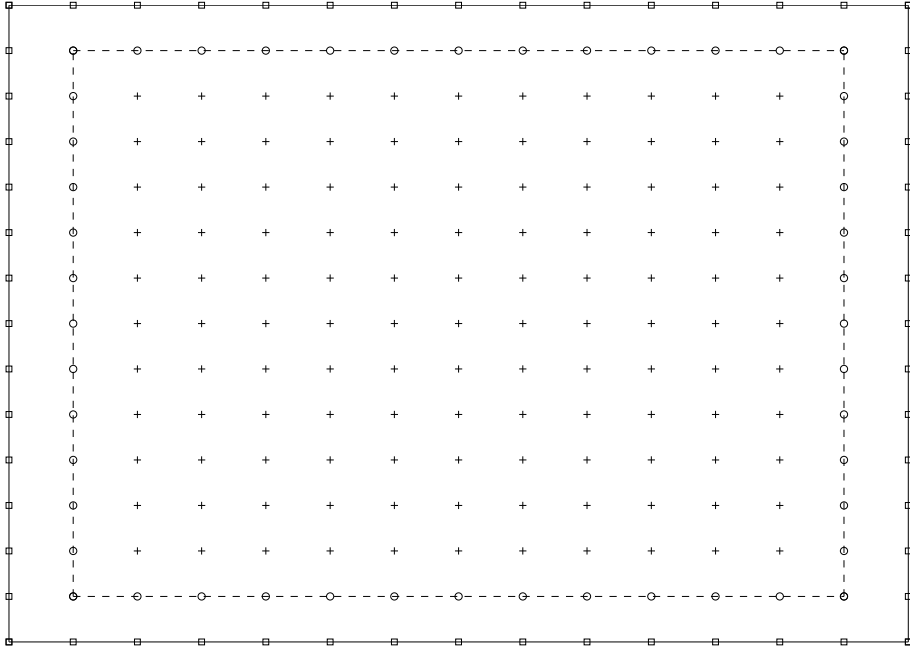
Figure 1: A problem domain and a typical discretisation. Legends square, circle and plus are used to denote the boundary nodes, the interior nodes next the boundary and the remaining interior nodes, respectively.

of zeros, respectively; equations $\widehat{u} = \mathcal{H}_x^{(0)} \widehat{w}_x$ are employed to collocate the variable u over the stencil; equations $\mathcal{H}_x^{(0)} \widehat{w}_x - \mathcal{H}_y^{(0)} \widehat{w}_y = \widehat{0}$ are employed to enforce nodal values of u obtained from the integration with respect to x and y to be identical; and equations $\mathcal{K}_x \widehat{w}_x + \mathcal{K}_y \widehat{w}_y = \widehat{e}$ are employed to represent extra information that can be values of the PDE (20) at selected nodes on the stencil and first-order derivative boundary conditions. In (35), $\mathcal{C}$ is the conversion matrix, $\widehat{u}$ and $\widehat{0}$ are vectors of length 25; $(\widehat{w}_x, \widehat{w}_y)^T$ is the RBF coefficient vector of length 90, and $\mathcal{O}, \mathcal{H}_x^{(0)}, \mathcal{H}_y^{(0)}, \mathcal{K}_x$ and $\mathcal{K}_y$ are matrices (the first three are of dimensions 25×45, while for the last two, their dimensions are dependent on the number of extra information values imposed and typically vary between 4×45 to 6×45). Solving (35) yields

$$\begin{pmatrix} \widehat{w}_x \\ \widehat{w}_y \end{pmatrix} = \mathcal{C}^{-1} \begin{pmatrix} \widehat{u} \\ \widehat{0} \\ \widehat{e} \end{pmatrix}. \tag{36}$$

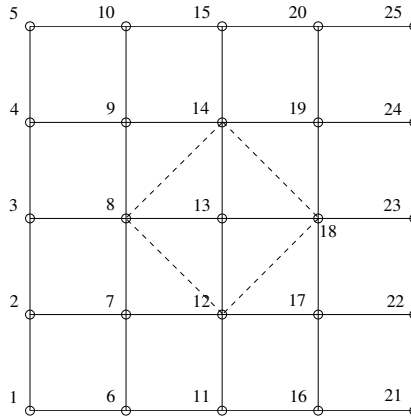Figure 2: A schematic representation of the proposed 5×5-node stencil associated with node (i, j). Over the stencil, nodes are locally numbered for bottom to top and left to right, where $13 \equiv (i, j)$. Nodal values of the governing equation used as extra information are placed on a diamond shape.

We present two ways, namely Implementation 1 and Implementation 2, to form the final set of algebraic equations.

Implementation 1: The final system is composed of two sets of equations. The first set is obtained by collocating the PDE at interior nodes (i, j) with ($3 \leq i \leq n_x - 2$ and $3 \leq j \leq n_y - 2$) and the second set is obtained by imposing first derivative boundary conditions at boundary nodes ($i = 1$, $2 \leq j \leq n_y - 1$), ($i = n_x$, $2 \leq j \leq n_y - 1$), ($3 \leq i \leq n_x - 2$, $j = 1$) and ($3 \leq i \leq n_x - 2$, $j = n_y$).

Implementation 2: First derivative boundary conditions are incorporated into the conversion system and the final system is formed by collocating the PDE only at all interior nodes.

Some implementation notes:

1. In constructing the approximations for stencils, the cross derivative $\partial^4 u / \partial x^2 \partial y^2$ is computed through the following relation [Mai-Duy and Tanner (2005a)], which

requires the approximation of second-order pure derivatives only,

$$
\frac{\partial^4 u}{\partial^2 x \partial^2 y} = \frac{1}{2} \left(\frac{\partial^2}{\partial x^2} \left(\frac{\partial^2 u}{\partial y^2} \right) + \frac{\partial^2}{\partial y^2} \left(\frac{\partial^2 u}{\partial x^2} \right) \right)
$$

$$
= \frac{1}{2} \left(\mathscr{H}_x^{(2)} \left[\mathscr{H}_x^{(0)} \right]^{-1} \left(\mathscr{H}_y^{(2)} \widehat{w}_y \right) + \mathscr{H}_y^{(2)} \left[\mathscr{H}_y^{(0)} \right]^{-1} \left(\mathscr{H}_x^{(2)} \widehat{w}_x \right) \right). \quad (37)
$$

2. For stencils whose central points are interior nodes (i, j) with $3 < i < n_x - 2$ and $3 < j < n_y - 2$, we construct $\widehat{e} = \mathscr{K}_x \widehat{w}_x + \mathscr{K}_y \widehat{w}_y$ through the collocation of the PDE (34) at four nodes placed in the diamond (i.e $(i-1, j), (i, j-1), (i, j+1)$ and $(i+1, j)$) as shown in Figure 2. The extra information vector can thus be expressed in the form

$$
\begin{pmatrix} f(\mathbf{x}_8) \\ f(\mathbf{x}_{12}) \\ f(\mathbf{x}_{14}) \\ f(\mathbf{x}_{18}) \end{pmatrix} = \begin{bmatrix} \mathscr{G}_x(8,:), \mathscr{G}_y(8,:) \\ \mathscr{G}_x(12,:), \mathscr{G}_y(12,:) \\ \mathscr{G}_x(14,:), \mathscr{G}_y(14,:) \\ \mathscr{G}_x(18,:), \mathscr{G}_y(18,:) \end{bmatrix} \begin{pmatrix} \widehat{w}_x \\ \widehat{w}_y \end{pmatrix}, \quad (38)
$$

where

$$
\mathscr{G}_x = \mathscr{H}_x^{(4)} + \mathscr{H}_y^{(2)} \left[\mathscr{H}_y^{(0)} \right]^{-1} \mathscr{H}_x^{(2)},
$$

and

$$
\mathscr{G}_y = \mathscr{H}_y^{(4)} + \mathscr{H}_x^{(2)} \left[\mathscr{H}_x^{(0)} \right]^{-1} \mathscr{H}_y^{(2)}.
$$

3. For stencils whose central points are $(3,3), (3, n_y - 2), (n_x - 2, 3)$ and $(n_x - 2, n_y - 2)$, the extra information vector is comprised of four nodal values of the derivative boundary condition and two nodal values of the PDE. For example, in the case of $(3,3)$, we form $\widehat{e} = \mathscr{K}_x \widehat{w}_x + \mathscr{K}_y \widehat{w}_y$ as

$$
\begin{pmatrix} \dfrac{\partial u(\mathbf{x}_2)}{\partial x} \\ \dfrac{\partial u(\mathbf{x}_3)}{\partial x} \\ \dfrac{\partial u(\mathbf{x}_6)}{\partial y} \\ \dfrac{\partial u(\mathbf{x}_{11})}{\partial y} \\ f(\mathbf{x}_{14}) \\ f(\mathbf{x}_{18}) \end{pmatrix} = \begin{bmatrix} \mathscr{H}_x^{(1)}(2,:), & \mathscr{O} \\ \mathscr{H}_x^{(1)}(3,:), & \mathscr{O} \\ \mathscr{O}, & \mathscr{H}_y^{(1)}(6,:) \\ \mathscr{O}, & \mathscr{H}_y^{(1)}(11,:) \\ G_x(14,:), & G_y(14,:) \\ G_x(18,:), & G_y(18,:) \end{bmatrix} \begin{pmatrix} \widehat{w}_x \\ \widehat{w}_y \end{pmatrix}. \quad (39)
$$

4. For stencils whose central points are $(i = 3, \ 3 < j < n_y - 2), (i = n_x - 2, \ 3 < j < n_y - 2), (3 < i < n_x - 2, \ j = 3)$ and $(3 < i < n_x - 2, \ j = n_y - 2)$, the extra information vector is comprised of one nodal value of the derivative boundary condition and

three nodal values of the PDE. For example, in the case of ($i = 3$, $3 < j < n_y - 2$), we form $\widehat{e} = \mathscr{K}_x \widehat{w}_x + \mathscr{K}_y \widehat{w}_y$ as

$$
\begin{pmatrix}
\dfrac{\partial u(\mathbf{x}_3)}{\partial x} \\
f(\mathbf{x}_{12}) \\
f(\mathbf{x}_{14}) \\
f(\mathbf{x}_{18})
\end{pmatrix}
=
\begin{bmatrix}
\mathscr{H}_x^{(1)}(3,:), & \mathscr{O} \\
G_x(12,:), & G_y(12,:) \\
G_x(14,:), & G_y(14,:) \\
G_x(18,:), & G_y(18,:)
\end{bmatrix}
\begin{pmatrix}
\widehat{w}_x \\
\widehat{w}_y
\end{pmatrix}.
\tag{40}
$$

Both Implementation 1 and Implementation 2 lead to a final system matrix of dimensions $(n_x - 2)(n_y - 2) \times (n_x - 2)(n_y - 2)$.

4.2 Compact local 13-node stencil (13-node CLS)

Figure 3 shows a schematic outline of a compact local 13-node stencil. The construction of the final system matrix using 13-node CLS is similar to that with 5×5-node CLS. Since the present stencil involves 13 nodes rather than 25 nodes, a sparse level (i.e. the number of zero entries) of the system matrix increases and its solution is thus more efficient. However, one can expect that 13-node CLS is less accurate than 5×5-node CLS.

4.3 Compact local 3×3-node stencil (3×3-node CLS)

A 3×3-node CLS is constructed through a coupled set of two Poisson equations

$$
\frac{\partial^2 v}{\partial x^2} + \frac{\partial^2 v}{\partial y^2} = f(x, y),
\tag{41}
$$

$$
\frac{\partial^2 u}{\partial x^2} + \frac{\partial^2 u}{\partial y^2} = v,
\tag{42}
$$

which represent the biharmonic equation (34).

Consider a grid node (i, j) ($2 \leq i \leq n_x - 1, 2 \leq j \leq n_y - 1$) and its associated 3×3-node stencil $\begin{bmatrix} \mathbf{x}_3 & \mathbf{x}_6 & \mathbf{x}_9 \\ \mathbf{x}_2 & \mathbf{x}_5 & \mathbf{x}_8 \\ \mathbf{x}_1 & \mathbf{x}_4 & \mathbf{x}_7 \end{bmatrix}$ $((i, j) \equiv \mathbf{x}_5)$.

4.3.1 Discretisation of equation (41)

Over a 3×3-node stencil, we construct the conversion system as

$$
\begin{pmatrix}
\widehat{v} \\
\widehat{0} \\
\widehat{e}^{[v]}
\end{pmatrix}
=
\underbrace{
\begin{bmatrix}
\mathscr{H}_x^{(0)}, & \mathscr{O} \\
\mathscr{H}_x^{(0)}, & -\mathscr{H}_y^{(0)} \\
\mathscr{K}_x^{[v]}, & \mathscr{K}_y^{[v]}
\end{bmatrix}
}_{\mathscr{C}^{[v]}}
\begin{pmatrix}
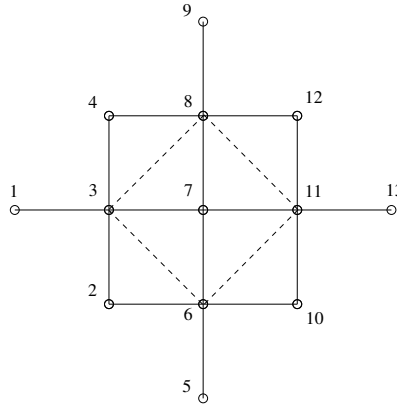\widehat{w}_x^{[v]} \\
\widehat{w}_y^{[v]}
\end{pmatrix},
\tag{43}
$$

Figure 3: A schematic representation of the proposed 13-node stencil associated with node (i, j). Over the stencil, nodes are locally numbered for bottom to top and left to right, where $7 \equiv (i, j)$. Nodal values of the governing equation used as extra information are placed on a diamond shape.

where $\widehat{v}$ and $\widehat{0}$ are vectors of length 9, $(\widehat{w}_x^{[v]}, \widehat{w}_y^{[v]})^T$ is the vector of length 30, $\mathscr{H}_x^{(0)}, \mathscr{H}_y^{(0)}$ are the matrices of dimensions 9×15, and equations $\widehat{e}^{[v]} = \mathscr{K}_x^{[v]} \widehat{w}_x^{[v]} + \mathscr{K}_y^{[v]} \widehat{w}_y^{[v]}$ can be used to represent extra information. Like 3-node CLS for 1D problems, we study here two cases of $\widehat{e}^{[v]}$. For the first case, the vector $\widehat{e}^{[v]}$ is used to represent nodal values of the governing equation at the four nodes $\mathbf{x}_1$, $\mathbf{x}_3$, $\mathbf{x}_7$ and $\mathbf{x}_9$. Hereafter, this stencil is referred to as 3×3-node CLS with GE. For the second case, the vector $\widehat{e}^{[v]}$ is set to null. Hereafter, this stencil is referred to as 3×3-node CLS without GE.

A mapping from the physical space into the RBF-coefficient space is obtained by solving (43)

$$\begin{pmatrix} \widehat{w}_x^{[v]} \\ \widehat{w}_y^{[v]} \end{pmatrix} = (\mathscr{C}^{[v]})^{-1} \begin{pmatrix} \widehat{v} \\ \widehat{0} \\ \widehat{e}^{[v]} \end{pmatrix}. \tag{44}$$

Making use of (44), one can express the PDE (41) at the central point of the stencil

as

$$\underbrace{\left[\mathscr{H}_x^{(2)}(5,:), \quad \mathscr{H}_y^{(2)}(5,:) \right] \left(\mathscr{C}^{[v]} \right)^{-1}}_{\mathscr{D}^{[v]}} \begin{pmatrix} \widehat{v} \\ \widehat{0} \\ \widehat{e}^{[v]} \end{pmatrix} = f(\mathbf{x}_5). \tag{45}$$

It can reduce to

$$\mathscr{D}_1^{[v]}\widehat{v} + \mathscr{D}_2^{[v]}\widehat{e}^{[v]} = f(\mathbf{x}_5), \tag{46}$$

where $\mathscr{D}_1^{[v]}$ and $\mathscr{D}_2^{[v]}$ are the first 9 entries and the last 4 entries of $\mathscr{D}^{[v]}$, respectively. In (46), $\mathscr{D}_2^{[v]}\widehat{e}_v$ and $f(\mathbf{x}_5)$ are known values.

4.3.2   Discretisation of equation (42)

Unlike equation (41), we consider nodal values of the field variable at grid nodes, $\partial u/\partial x$ at $\mathbf{x}_2$ and $\mathbf{x}_8$, and $\partial u/\partial y$ at $\mathbf{x}_4$ and $\mathbf{x}_6$ as unknowns in the discretisation of (42). The conversion matrix is thus formed as

$$\begin{pmatrix} \widehat{u} \\ \widehat{0} \\ \widehat{\partial u_x} \\ \widehat{\partial u_y} \end{pmatrix} = \underbrace{\begin{bmatrix} \mathscr{H}_x^{(0)}, & \mathscr{O} \\ \mathscr{H}_x^{(0)}, & -\mathscr{H}_y^{(0)} \\ \mathscr{H}_x^{(1)}([2,8],:), & \mathscr{O} \\ \mathscr{O}, & \mathscr{H}_y^{(1)}([4,6],:) \end{bmatrix}}_{\mathscr{C}^{[u]}} \begin{pmatrix} \widehat{w}_x^{[u]} \\ \widehat{w}_y^{[u]} \end{pmatrix}, \tag{47}$$

where $\widehat{\partial u_x} = (\partial u(\mathbf{x}_2)/\partial x, \partial u(\mathbf{x}_8)/\partial x)^T$ and $\widehat{\partial u_y} = (\partial u(\mathbf{x}_4)/\partial y, \partial u(\mathbf{x}_6)/\partial y)^T$. It is noted that the present additional unknowns $\widehat{\partial u_x}$ and $\widehat{\partial u_y}$ are defined and located in the same way as in the FDM work [Stephenson (1984)].

Solving (47) results in

$$\begin{pmatrix} \widehat{w}_x^{[u]} \\ \widehat{w}_y^{[u]} \end{pmatrix} = \left(\mathscr{C}^{[u]} \right)^{-1} \begin{pmatrix} \widehat{u} \\ \widehat{0} \\ \widehat{\partial u_x} \\ \widehat{\partial u_y} \end{pmatrix}. \tag{48}$$

Equation (48) can be split into

$$\widehat{w}_x^{[u]} = \left(\mathscr{C}_x^{[u]} \right)^{-1} \left(\widehat{u}, \quad \widehat{0}, \quad \widehat{\partial u_x}, \quad \widehat{\partial u_y} \right)^T, \tag{49}$$

$$\widehat{w}_y^{[u]} = \left(\mathscr{C}_y^{[u]} \right)^{-1} \left(\widehat{u}, \quad \widehat{0}, \quad \widehat{\partial u_x}, \quad \widehat{\partial u_y} \right)^T, \tag{50}$$

where $(\mathscr{C}_x^{[u]})^{-1}$ and $(\mathscr{C}_y^{[u]})^{-1}$ are the first and the last 15 rows of $(\mathscr{C}^{[u]})^{-1}$.

Through (49) and (50), the first derivatives of u at the central point of the stencil can be computed by

$$\frac{\partial u(\mathbf{x}_5)}{\partial x} = \mathscr{H}_x^{(1)}(5,:) \left(\mathscr{C}_x^{[u]}\right)^{-1} \begin{pmatrix} \widehat{u} \\ \widehat{0} \\ \widehat{\partial u_x} \\ \widehat{\partial u_y} \end{pmatrix}, \tag{51}$$

$$\frac{\partial u(\mathbf{x}_5)}{\partial y} = \mathscr{H}_y^{(1)}(5,:) \left(\mathscr{C}_y^{[u]}\right)^{-1} \begin{pmatrix} \widehat{u} \\ \widehat{0} \\ \widehat{\partial u_x} \\ \widehat{\partial u_y} \end{pmatrix}. \tag{52}$$

Through (48), the discrete form of equation (42) over the stencil can be written as

$$\underbrace{\left[\; \mathscr{H}_x^{(2)}, \quad \mathscr{H}_y^{(2)} \;\right] \left(\mathscr{C}^{[u]}\right)^{-1}}_{\mathscr{D}^{[u]}} \begin{pmatrix} \widehat{u} \\ \widehat{0} \\ \widehat{\partial u_x} \\ \widehat{\partial u_y} \end{pmatrix} = \widehat{v}. \tag{53}$$

Substitution of (53) into (46) leads to a discrete form of the biharmonic equation (34) at the central point of the stencil

$$\mathscr{D}_1^{[v]} \mathscr{D}^{[u]} \begin{pmatrix} \widehat{u} \\ \widehat{0} \\ \widehat{\partial u_x} \\ \widehat{\partial u_y} \end{pmatrix} = f(\mathbf{x}_5) - \mathscr{D}_2^{[v]} \widehat{f}_k. \tag{54}$$

By applying (51), (52) and (54) at every interior node, we will obtain the final system matrix of dimensions $3(n_x - 2)(n_y - 2) \times 3(n_x - 2)(n_y - 2)$.

It can be seen that the proposed compact local IRBF stencil does not require the calculation of cross derivatives explicitly. Furthermore, there is no need to derive a computational boundary condition for the intermediate variable v. When applying the proposed 3×3-node CLS to fluid flow problems, the variables u and v are replaced with the streamfunction and the vorticity variables, respectively.

5 Numerical examples

The accuracy of the solution is measured using the relative discrete L_2 norm

$$Ne(u) = \frac{\sqrt{\sum\limits_{i=1}^{n} (u_i - u_i^e)^2}}{\sqrt{\sum\limits_{i=1}^{n} (u_i^e)^2}}, \tag{55}$$

where n is the number of collocation nodes, and u_i and u_i^e are the computed and exact solutions, respectively.

We will study the behavior of the solution u with respect to (i) the grid size h, and (ii) the MQ width β.

5.1 One-dimensional problem

Consider the following fourth-order ODE

$$\frac{d^4 u}{dx^4} + \frac{d^2 u}{dx^2} = 16\pi^4 \sinh(2\pi x) + 4\pi^2 \sinh(2\pi x), \quad 0 \le x \le 2. \tag{56}$$

Double boundary conditions are defined as $u = 0$ and $du/dx = 2\pi$ at $x = 0$, and $u = 0$ and $du/dx = 2\pi \cosh(4\pi)$ at $x = 2$. The exact solution to this problem can be verified to be $u^e(x) = \sinh(2\pi x)$.

We employ 5-node CLS and 3-node CLS without and with GE to discretise (56). To assess the performance of the proposed stencils, the standard local 5-node IRBF stencil is also implemented. We conduct the calculations with several uniform grids, $(7, 9, \cdots, 37)$.

Figure 4 displays the solution accuracy and the matrix condition numbers against the grid size h. In terms of accuracy (Figure 4a), the solution converges apparently as $O(h^{1.40})$ for local 5-node stencil, and $O(h^{5.45})$, $O(h^{3.96})$ and $O(h^{4.16})$ for 5-node CLS and 3-node CLS without and with GE, respectively. The compact forms, even for the case of 3-nodes, thus outperform the standard form of 5 nodes as indicated by not only the norm error but also the convergence rate. It can be also seen that 3-node CLS with GE is more accurate than that without GE. In terms of the matrix condition number (Figure 4b), the 5-node CLS and the standard 5-node stencil yield similar values. It can be also seen that the inclusion of first derivatives in the IRBF approximations, i.e 3-node CLSs, leads to higher condition numbers of the system matrix.

Figure 5a shows a comparison of the accuracy between Implementation 1 and Implementation 2 for the case of 5-node CLS, indicating that both implementations
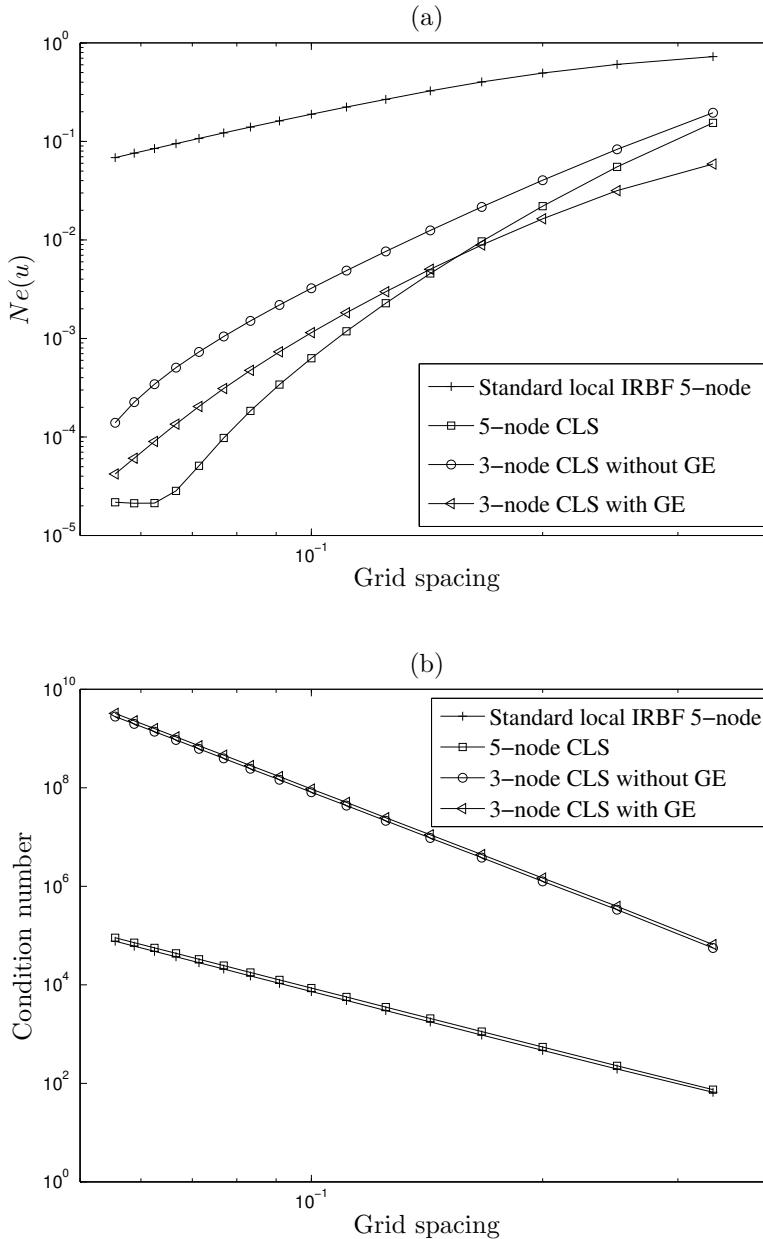
Figure 4: ODE: Relative L_2 errors of the solution u and condition numbers of the system matrix against the grid size by the proposed stencils and the standard local IRBF one. It is noted that we employ β=24 for local and compact local 5-node stencils, β=34 for 3-node CLS without GE, and β=5.6 for 3-node CLS with GE.
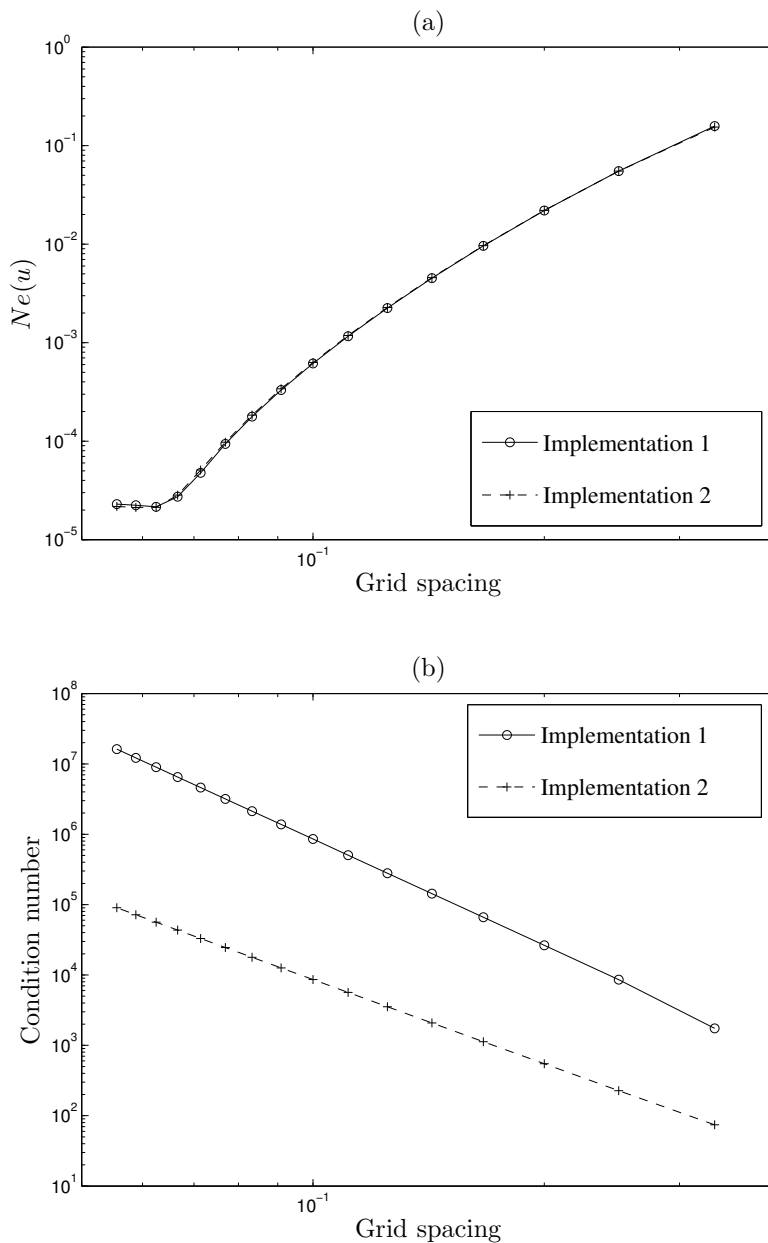
Figure 5: ODE, 5-node CLS, $\beta = 24$: The solution accuracy and matrix condition number against the grid size by Implementation 1 and Implementation 2.

give similar levels of accuracy. However, Figure 5b shows that Implementation 2 yields better condition numbers than Implementation 1, probably owing to the fact that the final system matrix of the former is composed of equations derived from the ODE only.

As mentioned earlier, the value of β would have a strong influence on the solution accuracy. Since the exact solution to this problem is available, it is straightforward to obtain the optimal value of β (i.e. at which $Ne(u)$ is minimum). Table 1 shows results obtained by a fixed value and the optimal value of β for three different grids. It can be seen that using the optimal value of β significantly enhances the solution accuracy.

5.2 *Two-dimensional problems*

5.2.1 *Example 1*

Consider the biharmonic problem with the source function

$$f(x,y) = 64\pi^4 \sin(2\pi x)\sin(2\pi y),$$

the domain of interest as $0 \le x, y \le 1$ and boundary conditions of the Dirichlet type. The exact solution is $u^e(x,y) = \sin(2\pi x)\sin(2\pi y)$.

Figure 6 shows the behaviour of the solution u using the proposed 13-node CLS ($\beta = 18$) with respect to the grid size h. Results obtained by the FD 13-node stencil are also included for comparison purposes. The IRBF method (Implementation 2) is much more accurate and converges much faster than the FDM (Figure 6a). The rate of convergence is 4.90 for the former and 1.99 for the latter. On the other hand, the IRBF matrix has higher condition numbers but grows slightly slower than the FD matrix (Figure 6b). The rate of growth is 3.25 for the former and 3.97 for the latter. Figure 7 indicates that Implementation 2 slightly outperforms Implementation 1 in terms of the matrix condition and accuracy. However, an improvement in the matrix condition here is not as significant as in the case of 1D problems.

Table 2 presents results by the proposed 5×5-node CLS for a fixed value and the optimal value of β. It can be seen that the MQ width has more influence on the solution accuracy than on the system matrix condition number. It is noted that a chosen fixed value $\beta = 2.5$ is the optimal value for the grid with $h = 1/50$.

Table 3 shows the accuracy and matrix condition number against the grid size by the proposed 3×3-node CLS without and with GE. The solution converges as $O(h^{3.36})$ for the former and $O(h^{3.88})$ for the latter. It can be seen that the incorporation of nodal values of the governing equation into the approximations results in an accuracy improvement.

Table 1: ODE, 5-node CLS, 3-node CLS with GE and 3-node CLS without GE: Relative L_2 errors of the solution u using some fixed and the optimal values of β for three grids.

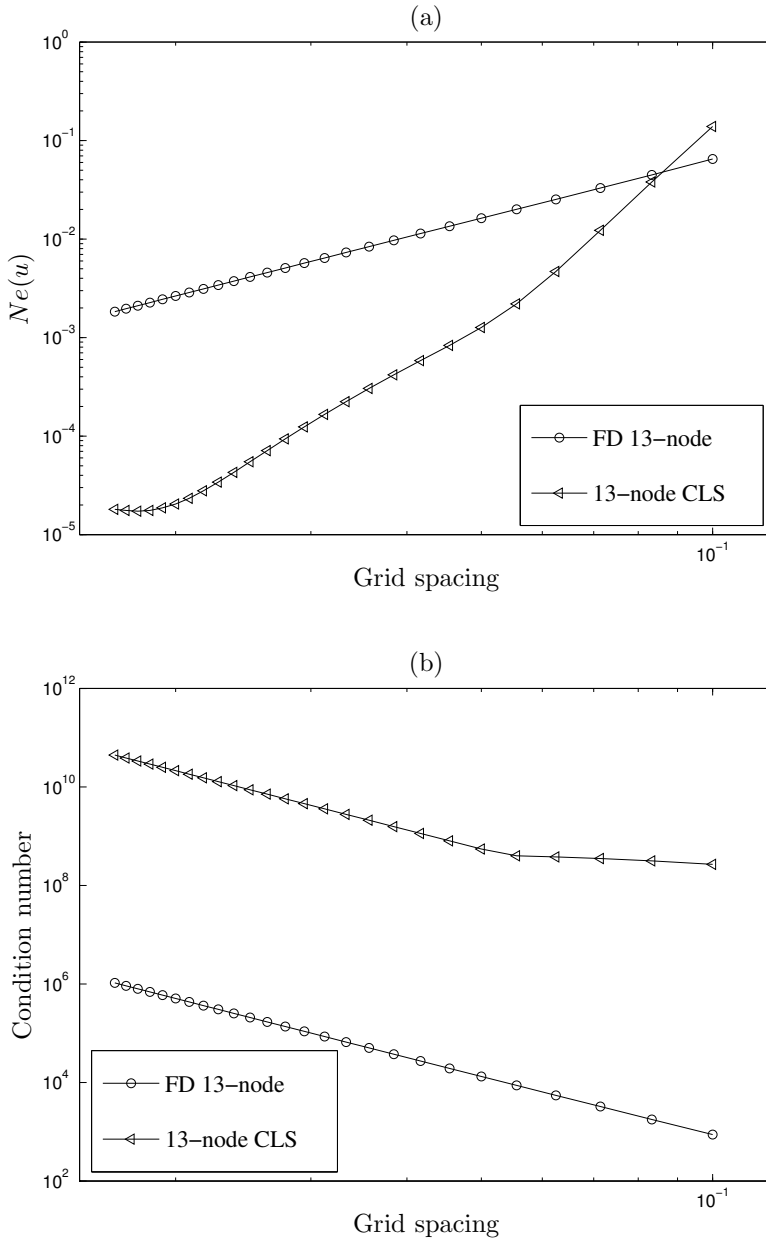| h	5-node CLS			3-node CLS					
				Without GE			With GE		
	Fixed β=24	Optimal β		Fixed β=77	Optimal β		Fixed β=10	Optimal β	
	$Ne(u)$	β	$Ne(u)$	$Ne(u)$	β	$Ne(u)$	$Ne(u)$	β	$Ne(u)$
1/20	6.30E-4	1.2	4.04E-4	3.46E-3	6	9.50E-4	1.60E-3	2.6	2.10E-4
1/50	1.59E-5	29.5	7.18E-6	5.85E-5	57	2.17E-5	2.31E-5	7	1.06E-5
1/70	6.39E-6	30.3	3.93E-7	8.22E-6	77	8.22E-6	2.97E-6	10	2.97E-6
	$O(h^{4.21})$			$O(h^{4.27})$			$O(h^{4.30})$		

Figure 6: PDE , Example 1, 13-node CLS, $\beta = 18$: The solution accuracy and matrix condition number against the grid size. Results by the FD 13-node stencil are also included.
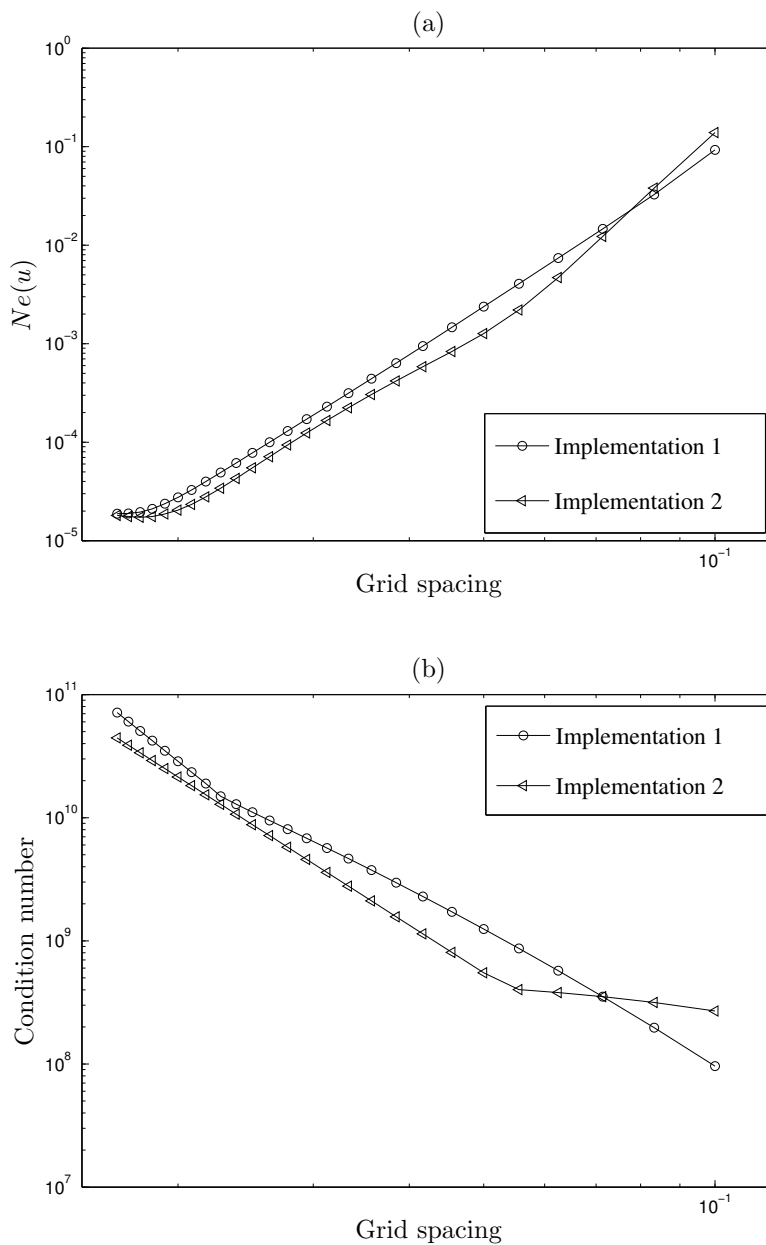
Figure 7: PDE, Example 1, 13-node CLS, $\beta = 18$: The solution accuracy and matrix condition number against the grid size by Implementation 1 and Implementation 2.

Table 2: PDE, Example 1, 5×5-node CLS: Condition numbers of the system matrix A and relative L_2 errors of the solution u using a fixed value and the optimal value of β for several grids.

	Fixed $\beta = 2.5$			Optimal β		
h	Cond(A)	$Ne(u)$	β	Cond(A)	$Ne(u)$
1/10	6.15E+2	1.54E-3	1	6.12E+2	1.44E-3
1/20	9.52E+3	1.65E-4	6.2	1.21E+4	7.59E-5
1/30	4.79E+4	8.24E-5	6.4	5.54E+4	1.34E-5
1/40	1.51E+5	4.41E-5	5	1.85E+5	1.35E-5
1/50	3.69E+5	6.47E-6	2.5	3.69E+5	6.47E-6
		$O(h^{3.04})$			$O(h^{3.34})$

5.2.2   *Example 2*

Among our proposed compact stencils, the 3×3-node CLS does not require special treatments for interior nodes close to the boundary. This stencil is applied here to obtain the structure of the steady-state lid-driven cavity flow in the streamfunction-vorticity formulation

$$\frac{\partial \psi}{\partial y} \frac{\partial \omega}{\partial x} - \frac{\partial \psi}{\partial x} \frac{\partial \omega}{\partial y} = \frac{1}{Re} \left(\frac{\partial^2 \omega}{\partial x^2} + \frac{\partial^2 \omega}{\partial y^2} \right), \tag{57}$$

$$-\omega = \frac{\partial^2 \psi}{\partial x^2} + \frac{\partial^2 \psi}{\partial y^2}, \tag{58}$$

where Re is the Reynolds number, ψ is the streamfunction and ω is the vorticity. One can compute the $x-$ and $y-$ velocity components according to the following definitions

$$u = \frac{\partial \psi}{\partial y} \text{ and } v = -\frac{\partial \psi}{\partial x}.$$

Table 3: PDE, Example 1, 3×3-node CLS: relative L_2 errors of the solution u for several grids.

h	Without GE, $\beta = 14.5$	With GE, $\beta = 16.6$
1/10	1.71E-02	1.29E-02
1/20	3.70E-03	3.43E-03
1/30	1.29E-03	1.23E-03
1/40	4.32E-04	4.05E-04
1/50	4.35E-05	8.13E-06
	$O(h^{3.36})$	$O(h^{3.88})$

The boundary conditions are prescribed in terms of the streamfunction as

$$\psi = 0, \quad \frac{\partial \psi}{\partial x} = 0 \quad \text{at x=0 and x=1,} \tag{59}$$

$$\psi = 0, \quad \frac{\partial \psi}{\partial y} = 0 \quad \text{at y=0,} \tag{60}$$

$$\psi = 0, \quad \frac{\partial \psi}{\partial y} = 1 \quad \text{at y=1.} \tag{61}$$

We employ several grids, $(21 \times 21, 31 \times 31, \cdots, 111 \times 111)$, in the simulation of the flow. A wide range of Re, $(0, 100, 400, 1000, 3200, 5000)$, is considered and the resultant nonlinear set of algebraic equations is solved using the Picard iteration scheme

$$\widehat{\theta} = \alpha \widehat{\theta}^{(k)} + (1 - \alpha) \widehat{\theta}^{(k-1)}, \tag{62}$$

where the superscript (k) is used to indicate the current iteration, α is the relaxation factor $(0 < \alpha \leq 1)$ and $\widehat{\theta} = (\widehat{\psi}, \widehat{\frac{\partial \psi}{\partial x}}, \widehat{\frac{\partial \psi}{\partial y}})^T$.

The flow is considered to reach a steady state when

$$\frac{\sqrt{\Sigma \left(\widehat{\boldsymbol{\theta}}^{(k)} - \widehat{\boldsymbol{\theta}}^{(k-1)} \right)^2}}{\sqrt{\Sigma \left(\widehat{\boldsymbol{\theta}}^{(k)} \right)^2}} < 10^{-9}. \tag{63}$$

As shown in Section 4.3, the proposed formulation does not require the derivation of a computational boundary condition for the vorticity and nodal values of the velocity components are obtained directly from solving the final system.

The value of β is chosen to be 20 for all simulations, while the value of α is employed in the range of 0.8 to 10^{-5}. The higher the value of Re the smaller the value of α will be.
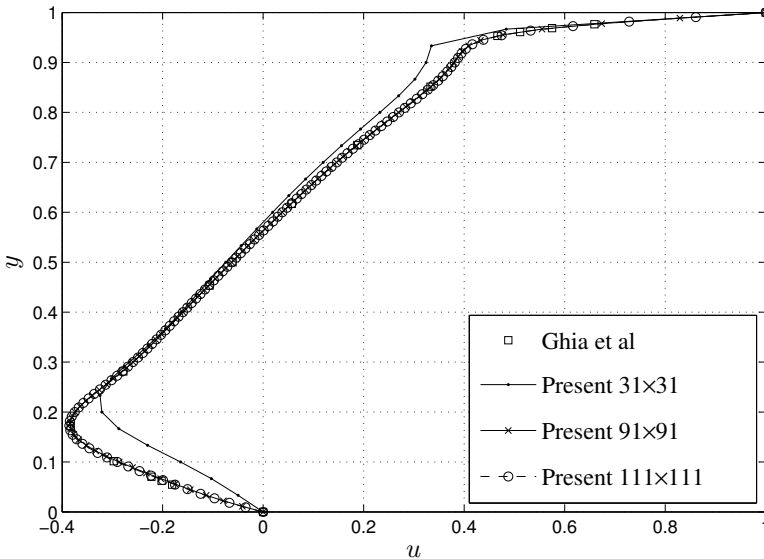
Figure 8: PDE, Example 2, $Re = 1000$: Profiles of the x−component of the velocity vector along the vertical centerline for several grids. Results by the FDM Ghia, Ghia, and Shin (1982) are also included.

The profile of the x−component of the velocity vector along the vertical centreline and of the y−component along the horizontal centreline for $Re = 1000$ using several grids are demonstrated in Figure 8 and Figure 9, respectively. To provide the base for assessment, results obtained by the multi-grid FDM [Ghia, Ghia, and Shin
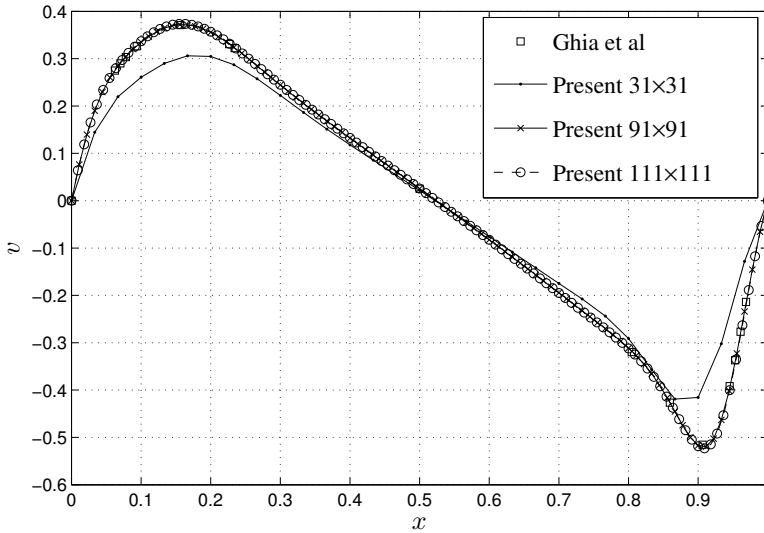
Figure 9: PDE, Example 2, $Re = 1000$: Profiles of the $y-$component of the velocity vector along the horizontal centerline for several grids. Results by the FDM Ghia, Ghia, and Shin (1982) are also included.

(1982)], which are widely cited in the literature, are included. It can be seen that a convergence with grid refinement is obtained for both velocity profiles.

Tables 4 and 5 give a comparison of the extreme values of the velocity profile on the centrelines obtained by the proposed method, FDM [Ghia, Ghia, and Shin (1982)], FVM [Deng, Piquet, Queutey, and Visonneau (1994)] and the pseudo-spectral method [Botella and Peyret (1998)]. It can be seen that the present results are in better agreement with the benchmark spectral solution than the others even for 'coarse' grids, e.g. 51×51 in the case of $Re = 100$ and 91×91 in the case of $Re = 1000$.

Results concerning the distribution of of the streamfunction and vorticity over the flow domain are shown in Figures 10 and 11, respectively. They look feasible in comparison with those in literature (e.g. [Ghia, Ghia, and Shin (1982); Botella and Peyret (1998); Deng, Piquet, Queutey, and Visonneau (1994)]).

6 Concluding Remarks

This paper is concerned with the development of several compact local IRBF stencils for solving fourth-order ODEs and PDEs. The IRBF approximations are ex-
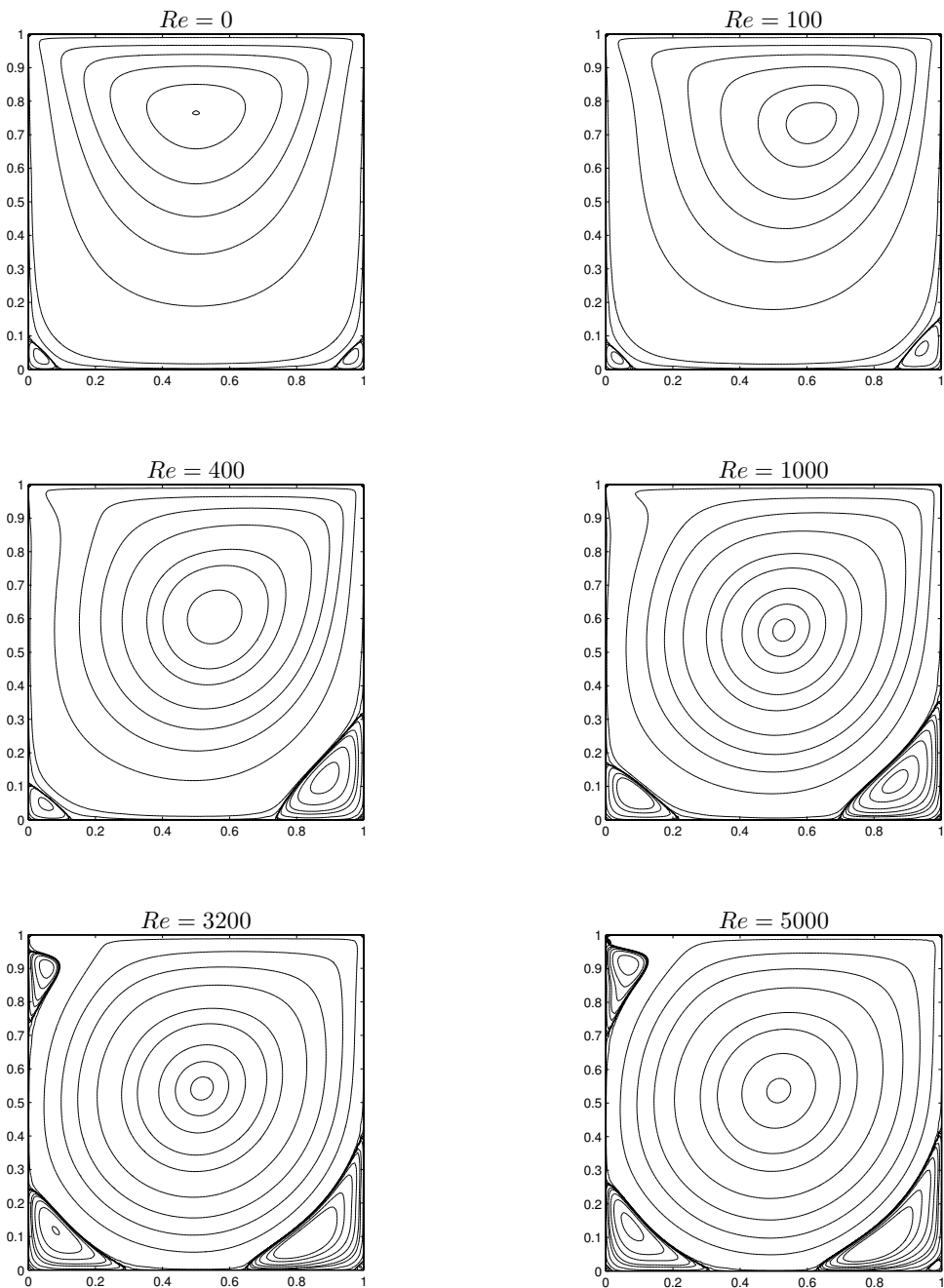
Figure 10: PDE, Example 2, 3×3-node CLS, a grid of 111×111: Streamlines of the flow at several Reynolds numbers. It can be seen that secondary vortices are clearly captured.
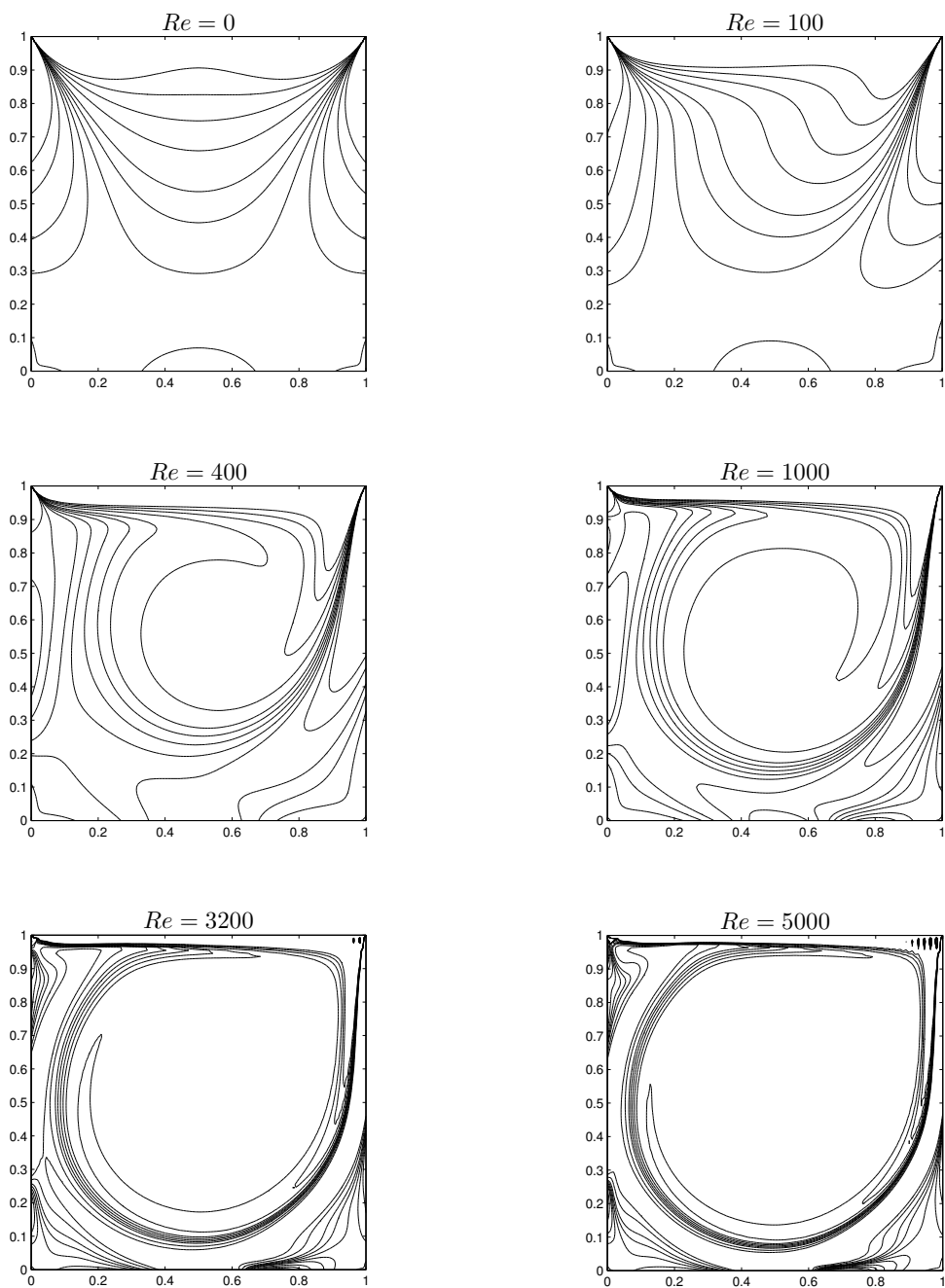
Figure 11: PDE, Example 2, 3×3-node CLS, a grid of 111×111: Iso-vorticity lines of the flow at several Reynolds numbers.

Table 4: PDE, Example 2, $Re = 100$, $\beta = 20$: Extreme values of the velocity profiles on the centerlines by the proposed method and several other methods. It is noted that N is the polynomial degree.

Reference	Grid	u_{max}	v_{max}	v_{min}
Present	31×31	0.21252	0.17675	-0.24908
Present	51×51	0.21354	0.17863	-0.25221
Present	71×71	0.21378	0.17910	-0.25302
Present	91×91	0.21386	0.17928	-0.25334
Present	111×111	0.21390	0.17937	-0.25350
FVM	64×64	0.21315	0.17896	-0.25339
FDM	129×129	0.21090	0.17527	-0.24533
Pseudo-spectral	$N = 96$	0.21404	0.17957	-0.25380

FVM, FDM and Pseudo-spectral refer to finite volume, finite difference and pseudo-spectral methods results in [Deng, Piquet, Queutey, and Visonneau (1994)], [Ghia, Ghia, and Shin (1982)], and [Botella and Peyret (1998)], respectively.

pressed in terms of not only nodal values of the field variable but also nodal values of the ODE/PDE and, in some cases, of first derivative(s). The latter is incorporated through the conversion system with the help of the integration constants. In the case of 3×3-node stencil, the resultant discretisation system is constructed through a set of two second-order PDEs, but there is no need to derive a computational boundary condition for the intermediate variable and no requirement for the calculation of cross derivatives explicitly. The proposed stencils are successfully verified using problems with analytic solution, showing that high rates of convergence and high levels of accuracy are obtained. For the lid-driven cavity flow, a convergent solution is obtained for high Re numbers and the obtained results are in very good agreement with the benchmark solutions.

Table 5: PDE, Example 2, $Re = 1000$, $\beta = 20$: Extreme values of the velocity profiles on the centerlines by the proposed method and several other methods. It is noted that N is the polynomial degree.

Reference	Grid	u_{max}	v_{max}	v_{min}
Present	31×31	0.32684	0.30773	-0.42971
Present	51×51	0.37061	0.35703	-0.50010
Present	71×71	0.38056	0.36802	-0.51530
Present	91×91	0.38411	0.37195	-0.52063
Present	111×111	0.38573	0.37376	-0.52305
FVM	128×128	0.38511	0.37369	-0.52280
FDM	129×129	0.38289	0.37095	-0.51550
Pseudo-spectral	$N = 96$	0.3885698	0.3796447	-0.5270771

FVM, FDM and Pseudo-spectral refer to finite volume, finite difference and pseudo-spectral methods results in [Deng, Piquet, Queutey, and Visonneau (1994)], [Ghia, Ghia, and Shin (1982)], and [Botella and Peyret (1998)], respectively.

References

Altas, I.; Dym, J.; Gupta, M.; Manohar, R. (1998): Multigrid solution of automatically generated high-order discretizations for the biharmonic equation. *SIAM Journal on Scientific Computing*, vol. 19, pp. 1575–1585.

An-Vo, D.-A.; Mai-Duy, N.; Tran-Cong, T. (2011): A C^2-continuous Control-Volume technique based on Cartesian grids and two-node integrated-RBF elements for second-order elliptic problems. *CMES: Computer Modeling in Engineering & Sciences*, vol. 72, pp. 299–334.

Bjørstad, P. (1983): Fast numerical solution of the biharmonic Dirichlet problem on rectangles. *SIAM Journal on Numerical Analysis*, vol. 20(1), pp. 59–71.

Botella, O.; Peyret, R. (1998): Benchmark spectral results on the Lid-driven cavity flow. *Computers & Fluids*, vol. 27, pp. 421–433.

Conte, S.; Dames, R. (1958): An alternating direction method for solving the biharmonic equation. *Mathematical Tables and Other Aids to Computation*, vol. 12 (63), pp. 198–205.

Deng, G.; Piquet, J.; Queutey, P.; Visonneau, M. (1994): Incompressible flow calculations with a consistent physical interpolation finite volume approach.

Computers & Fluids, vol. 23, pp. 1029–1047.

Franke, R. (1982): Scattered data interpolation: Tests of some methods. *Mathematics of Computation*, vol. 38 (157).

Ghia, U.; Ghia, K.; Shin, C. (1982): High-Re solutions for Incompressible flow using the Navier-Stokes equations and a multigrid method. *Journal of Computational Physics*, vol. 48, pp. 387–411.

Gupta, M.; Manohar, R. (1979): Direct solution of the bihramonic equations using noncoupled approach. *Journal of Computational Physics*, vol. 33, pp. 236–248.

Haykin, S. (1999): *Neural Networks: A Comprehensive Foundation (second Edition)*, volume 842. Prentice Hall.

Hughes, T. (1987): *The Finite Element Method: Linear Static and Dynamic Finite Element Analysis*. Prentice-Hall.

Kansa, E. (1990): Multiquadrics - A scattered data approximation scheme with applications to computational fluid-dynamics - I Surface approximations and partial derivative estimates. *Computers & Mathematics with Applications*, vol. 19(8-9), pp. 127–145.

Kansa, E. (1990): Multiquadrics - A scattered data approximation scheme with applications to computational fluid-dynamics - II Solutions to parabolic, hyperbolic and elliptic partial differential equations. *Computers & Mathematics with Applications*, vol. 19(8-9), pp. 147–161.

Kansa, E. (1999): Motivation for using radial basis functions to solve PDEs. *Mathematical Modelling and Industrial Mathematics Papers*, vol. 94551, pp. 1–8.

Mai-Duy, N. (2005): Solving high order ordinary differential equations with radial basis function networks. *International Journal for Numerical Methods in Engineering*, vol. 62(6), pp. 824–852.

Mai-Duy, N.; Tanner, R. (2005): Computing non-Newtonian fluid flow with radial basis function networks. *International Journal for Numerical Methods in Fluids*, vol. 48(12), pp. 1309–1336.

Mai-Duy, N.; Tanner, R. (2005): Solving high-order partial differential equations with indirect radial basis function networks. *International Journal for Numerical Methods in Engineering*, vol. 63(11), pp. 1636–1654.

Mai-Duy, N.; Tran-Cong, T. (2001): Numerical solution of differential equations using multiquadric radial basis function networks. *Neural Networks*, vol. 14, pp. 185–199.

Mai-Duy, N.; Tran-Cong, T. (2003): Approximation of function and its derivatives using radial basis function networks. *Applied mathematical modeling*, vol. 27, pp. 197–220.

Mai-Duy, N.; Tran-Cong, T. (2009): A Cartesian-grid discretisation scheme based on local integrated RBFNs for two-dimensional elliptic problems. *Computer Modeling in Engineering and Sciences*, vol. 51(3), pp. 213–238.

Mai-Duy, N.; Tran-Cong, T. (2010): A numerical study of 2D integrated RBFNs incorporating Cartesian grids for solving 2d elliptic differential problems. *Numerical methods for Partial Differential Equation*, vol. 26, pp. 1443–1462.

Mai-Duy, N.; Tran-Cong, T. (2011): Compact local integrated-RBF approximations for second-order elliptic differential problems. *Journal of Computational Physics*, vol. 230, pp. 4772–4794.

Ngo-Cong, D.; Mai-Duy, N.; Karunasena, W.; Tran-Cong, T. (2010): Free vibration analysis of laminated composite plates based on FSDT using one-dimensional IRBFN method. *Computers and Structures*, vol. 89(1-2), pp. 1–13.

Patankar, S. (1980): *Numerical Heat Transfer and Fluid Flow*. McGraw-Hill, New York.

Rannacher, R. (1999): Finite Element methods for the incompressible Navier-Stokes equations, 1999.

Reddy, J. (2005): *An introduction to the finite element method (Third Edition)*. McGraw-Hill.

Smith, G. (1978): *Numerical solution of partial differential equations: finite difference methods*. Oxford: Clarendon Press.

Stephenson, J. (1984): Single cell discretizations of order two and four for biharmonic problems. *Journal of Computational Physics*, vol. 55, pp. 65–88.